

Dynamics of a Bose-Einstein condensate in a symmetric triple-well trap

Thiago F Viscondi and K Furuya

Instituto de Física “Gleb Wataghin”, Universidade Estadual de Campinas - UNICAMP, 13083-859, Campinas, SP, Brazil

E-mail: viscondi@ifi.unicamp.br

Abstract. We present a complete analysis of the dynamics of a Bose-Einstein condensate trapped in a symmetric triple-well potential. Our classical analogue treatment, based on a time-dependent variational method using $SU(3)$ coherent states, includes the parameter dependence analysis of the equilibrium points and their local stability, which is closely related to the condensate collective behaviour. We also consider the effects of off-site interactions, and how these ‘cross-collisions’ may become relevant for a large number of trapped bosons. Besides, we have shown analytically, by means of a simple basis transformation in the single-particle space, that an integrable sub-regime, known as twin-condensate dynamics, corresponds in the classical phase space to invariant surfaces isomorphic to the unit sphere. However, the quantum dynamics preserves the twin-condensate defining characteristics only partially, thus breaking the invariance of the associated quantum subspace. Moreover, the periodic geometry of the trapping potential allowed us to investigate the dynamics of finite angular momentum collective excitations, which can be suppressed by the emergence of chaos. Finally, using the generalized purity associated to the $su(3)$ algebra, we were able to quantify the dynamical classicality of a quantum evolved system, as compared to the corresponding classical trajectory.

PACS numbers: 03.65.Sq, 03.75.Lm, 03.75.Kk

1. Introduction

The experimental observation of the Bose-Einstein condensation in systems of ultracold dilute alkali atomic clouds [1] has led to an active development of various studies concerning collective quantum phenomena. The special property of coherence presented in condensates of a large number of atoms allowed mean-field and semiclassical approaches to discover the fascinating dynamics of such a large quantum system.

The prospect of using magneto-optical traps with diverse confining geometries allowed the study of various quantum dynamical regimes, also including the possibility of testing the frontier between the quantum and classical mechanics through the increase of the total particle number to the macroscopic scale.

Several surveys have been performed in the case of a Bose-Einstein condensate trapped in a double well-potential under the two-mode approximation. Various subjects

were considered in these studies, such as tunneling dynamics [2], entanglement of modes [3] and quantum phase transition [4]. More recently the effects of the so-called *cross-collisions* have also been considered, and it was shown that these usually neglected higher order approximation terms can become quite important for large numbers of trapped bosons [5].

The dynamics of condensates in a triple-well potential has already been investigated a few times in the literature [6]. However, little attention has been paid to the specific case in which all three wells are identically coupled in pairs [7]. This arrangement is very interesting because it represents the simplest trapping potential where we can observe the rotation of the condensate.

In the present work we examine the dynamics of a condensate in a symmetric triple-well potential, under the three-mode approximation and considering the cross-collision terms. First, we investigate the classical analogue of the model and its phase space structure, by determining its fixed points and the Hamiltonian flow in the vicinity of these special solutions, which is closely related to the condensate collective excitations. Then, we choose the coherent states located in the proximity of the classical stationary states as initial quantum states. This enables us to capture in the *quantum dynamics* the characteristics associated to each of the classical fixed points. This strategy has been used before to observe the effect of chaos in the entanglement dynamics [8].

In section 2 we derive the model in the three-mode approximation, including the cross-collisional terms, and the corresponding Hamiltonian in terms of the SU(3) group generators. We also present the classical approximation based on the *time-dependent variational principle* (TDVP) [9] and the SU(3) coherent states [10]. The equilibrium points of the classical analogue equations of motion are divided into three classes: *twin-condensate states*, *single depleted well states* and *vortex states*. Here we show in detail the stability diagrams of the fixed points as functions of two collision parameters. The behaviour of the lowest energy fixed point and the occurrence of a quantum phase transition has been reported recently [11].

In section 3 we relate a simple permutation symmetry of the Hamiltonian to a transformation of the single-particle basis that leads to the twin-condensate subspace. Then, we demonstrate that the classically invariant subspace of twin-condensates is not fully preserved quantum mechanically. In addition, we compare the quantum population dynamics in the local modes with the corresponding classical evolution. Particularly interesting is the behaviour of the vortex states, for which we show the dynamics of a quantity associated with the condensate angular momentum along the symmetry axis of the trapping potential. The variation of the collision parameters can lead the vortex solutions to chaotic dynamics, and consequently inhibiting the condensate rotation in a preferred sense. It is notable that this model present chaotic behaviour at the classical level. Moreover, similarly to previous results for the double-well condensate model [4] with the measure known as *generalized purity* [12], we make a quantitative comparison between the quantum evolution and the classical approximation based on the coherent states. Section 4 is reserved to our conclusions and final considerations.

2. Model

Suppose a spinless boson of mass m trapped in a potential $V(\vec{r})$, whose equivalent minima are located at $\vec{r}_j = (x_j, y_j, 0)$, $j = 1, 2, 3$:

$$V(\vec{r}) = \frac{m\omega^2}{18q_0^4} \prod_{j=1}^3 [(x - x_j)^2 + (y - y_j)^2] + \frac{m\omega^2}{2} z^2. \quad (2.1)$$

Note that the potential is harmonic in z -direction with angular frequency ω and we choose $V(\vec{r}_j) = 0$. The parameter q_0 represents the distance between the potential minima and the origin of the coordinate system. For simplicity, we also choose $V(\vec{r})$ so that the harmonic approximation $V_j^{(2)}(\vec{r})$ around each minimum is isotropic with angular frequency ω . We can assign to each potential $V_j^{(2)}(\vec{r})$, taken independently, a localized ground state:

$$\langle \vec{r} | u_j \rangle = u_j(\vec{r}) = \frac{1}{\pi^{\frac{3}{4}} d^{\frac{3}{2}}} \exp \left[-\frac{(x - x_j)^2 + (y - y_j)^2 + z^2}{2d^2} \right]. \quad (2.2)$$

The Gaussian width is described by the parameter $d = \sqrt{\hbar/m\omega}$. Considering that $q_0 \gg d$, the states $|u_j\rangle$ are almost orthogonal, since $\varepsilon = \langle u_j | u_k \rangle = \exp[-3q_0^2/4d^2] \ll 1$, for $j \neq k$.

The states $|u_j\rangle$ are not eigenstates of the full single-particle Hamiltonian $H = \vec{p}^2/2m + V(\vec{r})$, but these localized states generate the same eigenspace of the three lowest energy states of H at first order in ε . That is, we have the following single-particle lowest energy states at $O(\varepsilon)$:

$$\begin{cases} |e_1\rangle = \frac{1}{\sqrt{3}} (|u_1\rangle + |u_2\rangle + |u_3\rangle) \\ |e_2\rangle = \frac{1}{\sqrt{6}} (|u_1\rangle + |u_2\rangle - 2|u_3\rangle) \\ |e_3\rangle = \frac{1}{\sqrt{2}} (|u_1\rangle - |u_2\rangle) \end{cases} \quad (2.3)$$

The states $|e_2\rangle$ and $|e_3\rangle$ are degenerated and the energy of these states differs from the energy of $|e_1\rangle$ by 3Ω , with the tunneling rate defined by:

$$\Omega \equiv \langle u_j | V(\vec{r}) - V_j^{(2)}(\vec{r}) | u_k \rangle + \varepsilon \frac{3\hbar\omega}{2}; \quad j \neq k. \quad (2.4)$$

Generally, for $q_0 \gg d$, Ω is negative and $|e_1\rangle$ is the single-particle ground state, whose energy difference for the next two states is proportional to ε .

So far we studied only the single-particle potential. Now, considering a system of N condensate bosons, we introduce the many-particle Hamiltonian:

$$\hat{H} = \int d^3r \hat{\psi}^\dagger(\vec{r}) H \hat{\psi}(\vec{r}) + \frac{1}{2} \int d^3r d^3r' \hat{\psi}^\dagger(\vec{r}) \hat{\psi}^\dagger(\vec{r}') \mathcal{V}(\vec{r}, \vec{r}') \hat{\psi}(\vec{r}') \hat{\psi}(\vec{r}). \quad (2.5)$$

where H is the single-particle Hamiltonian and $\mathcal{V}(\vec{r}, \vec{r}')$ is the pair interaction potential. Only pair interactions are significant, because we assume dilute condensate gas,

characterized by a high mean free path, which makes higher order collisions unlikely. For particles of momentum approaching zero, as in the case of a condensate, a good approximation for the interaction potential is the following effective potential [13]:

$$\mathcal{V}(\vec{r}, \vec{r}') = \frac{4\pi\hbar^2 a}{m} \delta(\vec{r} - \vec{r}') = V_0 \delta(\vec{r} - \vec{r}'). \quad (2.6)$$

In the previous equation we defined the s -wave scattering length, denoted by a . Now, supposing that the states of (2.3) are the only significantly populated, we get our second approximation in (2.5), namely, the *three-mode approximation*:

$$\hat{\psi}(\vec{r}) \approx \langle \vec{r} | u_1 \rangle a_1 + \langle \vec{r} | u_2 \rangle a_2 + \langle \vec{r} | u_3 \rangle a_3; \quad (2.7)$$

where we defined a_j as the annihilation operator for the state $|u_j\rangle$. Therefore, the field operator $\hat{\psi}(\vec{r})$ may be expanded in the local modes described in (2.2), which generate the same single-particle space as the energy states of (2.3). Substituting (2.6) and (2.7) in (2.5), we obtain the following Hamiltonian[‡], retaining only the terms up to order $\varepsilon^{\frac{3}{2}}$:

$$\hat{H} = \Omega' \sum_{j \neq k} a_j^\dagger a_k + \kappa \sum_j a_j^{\dagger 2} a_j^2 - 2\Lambda \widetilde{\sum_{j,k,m}} a_j^\dagger a_j a_k^\dagger a_m. \quad (2.8)$$

The third summation symbol in (2.8) indicates the sum over three different indices. In the previous equation we defined the effective tunneling rate $\Omega' = \Omega + 2\Lambda(N - 1)$ and the following collision parameters:

$$\begin{aligned} \kappa &= \frac{V_0}{2} \int d^3r u_j^4(\vec{r}) = \frac{V_0}{2^{\frac{5}{2}} \pi^{\frac{3}{2}} d^3}; \\ \Lambda &= \frac{V_0}{2} \int d^3r u_j^3(\vec{r}) u_k(\vec{r}) = \kappa \varepsilon^{\frac{3}{2}}; \quad j \neq k. \end{aligned} \quad (2.9)$$

The *self-collision rate* κ is proportional to the collision frequency between bosons in the same potential well, while the *cross-collision rate* Λ is proportional to the collision frequency between bosons coming from different local modes. Note that the effective tunneling rate Ω' depends on the cross-collision parameter and the total number of trapped bosons. Also, observe that we have $|\Lambda| \ll |\kappa|$ for $\varepsilon \ll 1$. Although the cross-collision rate has a lower order of magnitude than Ω , the product $N\Lambda$ in Ω' may be relevant for large numbers of trapped bosons. Therefore, the cross-collisions become important in comparing theoretical and experimental results, because they include significant effects of the number of particles in the effective tunneling rate.

Since \hat{H} conserves the total number of trapped particles under unitary evolution, we can use the following homomorphism between the bilinear bosonic operators and the generators of the SU(3) group:

$$\begin{aligned} Q_1 &= \frac{1}{2}(a_1^\dagger a_1 - a_2^\dagger a_2), & Q_2 &= \frac{1}{3}(a_1^\dagger a_1 + a_2^\dagger a_2 - 2a_3^\dagger a_3), \\ J_k &= i(a_k^\dagger a_j - a_j^\dagger a_k), & P_k &= a_k^\dagger a_j + a_j^\dagger a_k; \end{aligned} \quad (2.10)$$

[‡] Note that we use the bosonic canonical commutation relations to simplify the final expression for \hat{H} . We also discard the terms dependent only on the conserved total number of particles, as such terms do not change the system dynamics for a fixed value of N .

for $k = 1, 2, 3$ and $j = (k + 1) \bmod 3 + 1$. The Hamiltonian (2.8) can be rewritten in terms of the operators (2.10), characterizing SU(3) as the dynamical group of the system \S :

$$\begin{aligned} \hat{H} = & \left(\Omega' - 2\Lambda \frac{N}{3} \right) (P_1 + P_2 + P_3) + \frac{\kappa}{2} (4Q_1^2 + 3Q_2^2) \\ & + \Lambda [2Q_1(P_1 - P_3) + Q_2(2P_2 - P_1 - P_3)]. \end{aligned} \quad (2.11)$$

Notice that the tunneling term is linear in the SU(3) generators, while the collision terms are quadratic. Within the three-mode approximation, a single-particle operator A and its corresponding many-particle operator \hat{A} are related by:

$$\hat{A} = \sum_{j,k=1}^3 \langle u_j | A | u_k \rangle a_j^\dagger a_k. \quad (2.12)$$

Therefore, considering terms up to first order in ε , we can find relations between the generators of SU(3) and basic system observables. First, we have the following condensate position operators, obtained by choosing $\vec{r}_1 = \left(-\frac{1}{2}q_0, \frac{\sqrt{3}}{2}q_0, 0\right)$, $\vec{r}_2 = \left(-\frac{1}{2}q_0, -\frac{\sqrt{3}}{2}q_0, 0\right)$ and $\vec{r}_3 = (q_0, 0, 0)$:

$$\begin{aligned} \hat{x} = & -\frac{3q_0}{2}Q_2 + \frac{\varepsilon q_0}{2} \left[\frac{1}{2}(P_1 + P_3) - P_2 \right]; \\ \hat{y} = & \sqrt{3}q_0Q_1 + \frac{\sqrt{3}\varepsilon q_0}{4}(P_1 - P_3). \end{aligned} \quad (2.13)$$

The operators J_k , $k = 1, 2, 3$, generate a subalgebra of su(3) isomorphic to su(2), the angular momentum algebra. Nevertheless, linear combinations of these operators are directly proportional to the *linear momentum* operators of the condensate:

$$\begin{aligned} \hat{p}_x = & \frac{3\varepsilon q_0}{4d^2} (J_3 - J_1); \\ \hat{p}_y = & \frac{\sqrt{3}\varepsilon q_0}{4d^2} (J_1 + J_3 - 2J_2). \end{aligned} \quad (2.14)$$

However, the condensate *angular momentum* operator along the z-axis is proportional to the sum $J_S = J_1 + J_2 + J_3$:

$$\hat{L}_z = \frac{\sqrt{3}\varepsilon q_0^2}{4d^2} J_S. \quad (2.15)$$

2.1. Classical Approximation

Mean field theories and classical trajectories are used widely in the literature for the treatment of condensate dynamics. Here we introduce our classical approach to the problem based on the *time-dependent variational principle*. Considering independent variations in an arbitrary state $|\psi\rangle$ of Hilbert space and its conjugate $\langle\psi|$, it is known

\S Here again we discard some terms dependent only on the fixed total number of particles N .

that the extremization of the following action functional is equivalent to the Schrödinger equation \parallel :

$$S = \int_{t_i}^{t_f} dt \left[\frac{i}{2} \frac{\langle \dot{\psi} | \dot{\psi} \rangle - \langle \dot{\psi} | \psi \rangle}{\langle \psi | \dot{\psi} \rangle} - \frac{\langle \dot{\psi} | \hat{H} | \psi \rangle}{\langle \psi | \dot{\psi} \rangle} \right]. \quad (2.16)$$

We can make approximations to the Schrödinger equation by a suitable parametrization of the time dependence of the state $|\psi\rangle$, restricting the state evolution to a subspace of the Hilbert space. The classical approximation is achieved when the state is restricted to the nonlinear subspace constituted only by the coherent states associated with the dynamical group [9]. For the SU(3) bosonic representations, we have the following coherent states [10]:

$$\begin{aligned} |N; w_1, w_2\rangle &= \sum_{n_1+n_2+n_3=N} \left(\frac{N!}{n_1!n_2!n_3!} \right)^{\frac{1}{2}} \frac{w_1^{n_1} w_2^{n_2} |n_1, n_2, n_3\rangle}{(|w_1|^2 + |w_2|^2 + 1)^{\frac{N}{2}}} \\ &= \frac{1}{\sqrt{N!}} \left[\frac{w_1 a_1^\dagger + w_2 a_2^\dagger + a_3^\dagger}{\sqrt{|w_1|^2 + |w_2|^2 + 1}} \right]^N |0\rangle. \end{aligned} \quad (2.17)$$

The variables $w_1, w_2 \in \mathbb{C}$ parametrize the subspace composed of coherent states for a fixed number particles N . The states $\{|n_1, n_2, n_3\rangle\}$ form the basis of the three-mode bosonic Fock space, where $n_j \in \mathbb{N}$ is the occupation number associated with the local state $|u_j\rangle$. Applying the variational principle to the action functional (2.16) with $|\psi\rangle = |N; w_1, w_2\rangle$, we obtain the classical equations of motion for the complex variables w_j :

$$i\dot{w}_j = \frac{|w_1|^2 + |w_2|^2 + 1}{N} \left[(|w_j|^2 + 1) \frac{\partial \mathcal{H}}{\partial w_j^*} + w_j w_k^* \frac{\partial \mathcal{H}}{\partial w_k^*} \right]; \quad (2.18)$$

for $j, k = 1, 2$ and $k \neq j$. The quantity $\mathcal{H}(w_1^*, w_2^*, w_1, w_2)$ is the effective classical Hamiltonian, given by the average of \hat{H} in the coherent states:

$$\begin{aligned} \frac{\mathcal{H}}{N} &= \frac{\langle N; w_1, w_2 | \hat{H} | N; w_1, w_2 \rangle}{N} \\ &= \Omega \left\{ (1 + 2\mu) \frac{w_1^* w_2 + w_2^* w_1 + w_1 + w_1^* + w_2 + w_2^*}{1 + |w_1|^2 + |w_2|^2} + \chi \frac{(|w_1|^4 + |w_2|^4 + 1)}{(|w_1|^2 + |w_2|^2 + 1)^2} \right. \\ &\quad \left. - 2\mu \frac{[|w_1|^2(w_2^* + w_2) + |w_2|^2(w_1^* + w_1) + w_1^* w_2 + w_2^* w_1]}{(|w_1|^2 + |w_2|^2 + 1)^2} \right\}. \end{aligned} \quad (2.19)$$

In the previous equation we introduced new collision parameters, which allowed us to eliminate the dependence on N from the average energy per particle and also prevented us from problems of divergence in the macroscopic limit $N \rightarrow \infty$. The quantities χ and μ as functions of the old collision parameters are given by:

$$\chi = \frac{\kappa(N-1)}{\Omega}, \quad \mu = \frac{\Lambda(N-1)}{\Omega}. \quad (2.20)$$

\parallel In what follows we make $\hbar = 1$.

Note that $|\chi| \gg |\mu|$, because supposedly we have $|\kappa| \gg |\Lambda|$. Substituting the Hamiltonian (2.19) into (2.18), we obtain the classical equations of motion for the three-mode condensate:

$$i\dot{w}_j = \Omega \left\{ (1 + 2\mu)(1 - w_j)(w_j + w_k + 1) + 2\chi \frac{w_j(|w_j|^2 - 1)}{|w_j|^2 + |w_k|^2 + 1} - 2\mu \frac{[(1 - w_j)w_k^*(w_j + w_k + w_j w_k) - (1 + w_j)w_k(|w_j|^2 - 1)]}{|w_j|^2 + |w_k|^2 + 1} \right\}; \quad (2.21)$$

again for $j, k = 1, 2$ and $k \neq j$. The TDVP based classical approximation with coherent states is exact for any linear Hamiltonian in the dynamical group generators, i.e., the classical equations of motion (2.21) reproduce the correct quantum evolution of a coherent state in the case of non-interacting bosons, for $\chi = \mu = 0$. The approximation also becomes exact in the classical limit, which coincides with the macroscopic limit $N \rightarrow \infty$, since the total number of trapped bosons plays a role equivalent to the reciprocal of \hbar [14]. However, considering χ and μ as independent parameters, we see that the equations of motion (2.21) and the Hamiltonian per particle (2.19) are independent of N , and therefore represent the *exact results* in the classical-macroscopic limit.

The equations of motion (2.18) assume the canonical form under the following change of dynamical variables:

$$w_j = \left(\frac{K_j}{N - K_1 - K_2} \right)^{\frac{1}{2}} e^{-i\phi_j}; \quad (2.22)$$

for $j = 1, 2$. The canonical variables K_j and ϕ_j have an useful and immediate physical interpretation. The variable K_j is the mean bosonic occupation in the j -th potential well, and $(N - K_1 - K_2)$ is the mean population in the third well due to the conservation of the total number of particles. The angular variable ϕ_j represents the phase difference between the portions of the condensate located at the j -th and third wells.

2.2. Equilibrium Points

2.2.1. Twin-condensates According to the equations of motion (2.21), the classical phase space of the condensate has three invariant subspaces arising from the discrete rotational symmetry of the trapping potential, which are described by the following conditions:

$$w_1 = w_2, \quad w_1 = 1, \quad w_2 = 1. \quad (2.23)$$

Each one of these equivalent invariant subspaces follows from the equality in phase and mean occupation of a pair of local modes, according to the transformation (2.22). Therefore, if two localized condensates have the same initial classical state, so they remain identical during their classical evolution. This integrable sub-regime of the model is known as *twin-condensate dynamics*.

The majority of the equilibrium points of the equations of motion (2.21) are located in the twin-condensate subspaces under the additional constraint $w_1, w_2 \in \mathbb{R}$. Therefore, by making $w_1 = w_2 \in \mathbb{R}$ and $\dot{w}_j = 0$ in (2.21), we obtain the following polynomial equation for the location of the twin-condensate fixed points:

$$4(1 + \mu)w_1^4 - 2(1 + \chi + 4\mu)w_1^3 + 6\mu w_1^2 + (2\chi - 1)w_1 - 1 - 2\mu = 0. \quad (2.24)$$

The above equation clearly has the solution $w_1 = w_2 = 1$, regardless of the choice of the collision parameter values. This equilibrium point, according to the interpretation of the transformation (2.22), corresponds to the state with identical phase and mean occupation in all three local modes. We denote this solution by s_1 , which is the intersection of the three invariant surfaces in (2.23). Excluding the solution s_1 from (2.24), we obtain a cubic equation for the remaining real fixed points:

$$w_1^3 + \frac{(1 - \chi - 2\mu)}{2(1 + \mu)}w_1^2 + \frac{(1 - \chi + \mu)}{2(1 + \mu)}w_1 + \frac{(1 + 2\mu)}{4(1 + \mu)} = 0. \quad (2.25)$$

The number of real solutions of the equation (2.25) depends on the sign of the following discriminant:

$$\Delta = -\chi^4 - 2(3 + 7\mu)\chi^3 + 3(2 - 11\mu^2)\chi^2 + 2(5 + 12\mu - 18\mu^2 - 52\mu^3)\chi + 2(9 + 76\mu + 228\mu^2 + 264\mu^3 + 76\mu^4). \quad (2.26)$$

This discriminant has two real roots in χ , the positive (negative) root is denoted by $\chi_+(\mu)$ ($\chi_-(\mu)$). If $\chi_-(\mu) < \chi < \chi_+(\mu)$, the equation (2.25) has only one real solution that we denote by $s_2(\chi, \mu)$. However, for $\chi = \chi_{\pm}(\mu)$ we have a new equilibrium point, which undergoes a bifurcation for $\chi > \chi_+(\mu)$ and $\chi < \chi_-(\mu)$, giving rise to the solutions denoted by $s_3(\chi, \mu)$ and $s_4(\chi, \mu)$. Figure 1 shows the number of real solutions of equation (2.24) as a function of the collision parameters. Note that for $\chi = \frac{9}{4} + \mu$ we have only three real solutions to (2.24), because on this curve the solutions s_1 and $s_3(\chi, \mu)$ become degenerate.

By the linearization of the equations of motion (2.21), we can analyze the stability of the dynamics in the vicinity of each equilibrium point. Although the position of the equilibrium point s_1 does not depend on the collision parameters, we can show the following condition of stability for this equilibrium point:

$$\lambda_{s_1}^2 = \frac{|\Omega|^2}{3}(3 + 4\mu)(4\chi - 9 - 4\mu) < 0. \quad (2.27)$$

Therefore, considering $\mu > -\frac{3}{4}$, s_1 is stable for $\chi < \frac{9}{4} + \mu$. Note that this critical curve of stability change coincides with the curve of degeneracy of s_1 and $s_3(\chi, \mu)$.

The behaviour of the fixed point $s_2(\chi, \mu)$ as a function of the collision parameters is shown in figure 2.(a). Therefore, for $|\chi| \gg |\mu|$, s_2 is generally stable (unstable) for $\chi < 0$ ($\chi > 0$). Also for $|\chi| \gg |\mu|$, we can demonstrate that the equilibrium point s_3 (s_4) is unstable (stable) in its region of existence in the parameter space, thus characterizing a *saddle-node* bifurcation¶.

¶ We do not show the algebraic conditions of stability for s_2 , s_3 and s_4 because they are exceedingly long and complicated, due mostly to the position dependence of these equilibrium points on χ and μ .

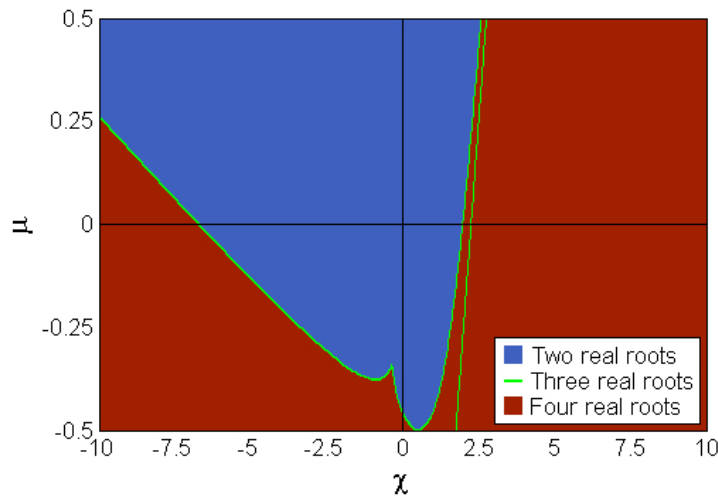


Figure 1. [colour] Number of real solutions of equation (2.24) as a function of the collision parameters. The light grey [green] curves represent the transitional situation of existence of only three real solutions. Note that only the quadrants where $\chi\mu > 0$ are physically accessible, since the two collision parameters must have the same sign.

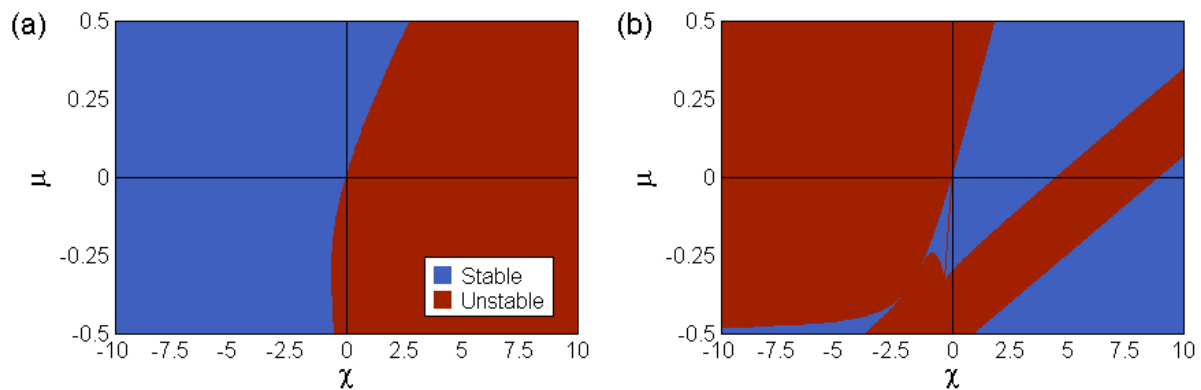


Figure 2. [colour] (a) Stability analysis of the equilibrium point $s_2(\chi, \mu)$ as a function of collision parameters. (b) Stability analysis of the single depleted well states. Note that these are unstable equilibrium points on the curve $\chi = \mu$.

2.2.2. Single Depleted Well States Returning to the equations of motion, we can find two more real equilibrium points with coordinates independent of the collision parameters:

$$w_j = -1, \quad w_k = 0; \quad (2.28)$$

for $j, k = 1, 2$ and $j \neq k$. The fixed points above are known as *single depleted well states*, and according to the transformation (2.22) they always possess one completely empty local mode, while the two other modes have opposite phases and the same average population⁺. The single depleted well states have the following stability conditions, also

⁺ The rotational symmetry of the trapping potential indicates the presence of a third single depleted well state, corresponding to the complete depletion of the third well. However, according to the transformations (2.22), this third equilibrium point would receive the coordinates $w_1, w_2 \rightarrow \infty$.

shown in figure 2.(b):

$$\lambda_{SDW,\pm}^2 = \frac{|\Omega|^2}{2} \left\{ -[9 + 4\mu(10 + 11\mu) + \chi(2 + \chi)] \pm [(9 + 16\mu - \chi) \times (9 + 128\mu^3 - 8\mu^2(\chi - 19) + \chi(5 + 3\chi - \chi^2) + 16\mu(4\chi + \chi^2))]^{\frac{1}{2}} \right\} < 0. \quad (2.29)$$

2.2.3. Vortex States Within the classical approximation, the angular momentum of the condensate along the symmetry axis of the trapping potential is proportional to:

$$\langle N; w_1, w_2 | J_S | N; w_1, w_2 \rangle = \frac{2N}{|w_1|^2 + |w_2|^2 + 1} \text{Im}(w_1 - w_2 + w_1^* w_2). \quad (2.30)$$

Therefore, the classical angular momentum is directly related to the imaginary parts of the variables w_1 and w_2 . Since all equilibrium points found previously have real coordinates, they represent irrotational condensate configurations. However, the equations (2.21) have a further pair of fixed points:

$$w_1 = e^{\pm i \frac{2\pi}{3}}, \quad w_2 = e^{\mp i \frac{2\pi}{3}}. \quad (2.31)$$

According to (2.22), these latter equilibrium points have the same mean occupation in all three local modes, since $|w_1| = |w_2| = 1$, but the phase difference between each pair of local condensates is $\pm \frac{2\pi}{3}$, which is the angle of rotational symmetry of the trapping potential. The states corresponding to (2.31) are known as vortex states, due to their nonzero angular momentum, which is proportional to the total number of condensate bosons:

$$\langle N; w_1 = w_2^* = e^{\pm i \frac{2\pi}{3}} | J_S | N; w_1 = w_2^* = e^{\pm i \frac{2\pi}{3}} \rangle = \pm \sqrt{3}N. \quad (2.32)$$

Note that the two vortex states are equivalent, because they differ only in their sense of rotation. The stability condition for the vortex states is given by:

$$\lambda_{V,\pm}^2 = \frac{|\Omega|^2}{6} \left[-104\mu^2 - 16\mu(6 + \chi) - 3(9 + 4\chi) \pm \sqrt{3(3 + 4\mu)(3 + 8\mu)^2(9 + 4\mu + 8\chi)} \right] < 0. \quad (2.33)$$

Therefore, considering $\mu > -\frac{3}{4}$, the vortex states are stable for $\chi \geq -(4\mu + 9)/8$, except on the curve $\chi = 2\mu(6 + 11\mu)/(3 + 4\mu)$.

3. Condensate Dynamics

3.1. Twin-condensate Dynamics

The integrable sub-regime of twin-condensates is a direct consequence of the symmetry of \hat{H} under the permutation of indices of the three local modes. The equivalence of the three local modes remains in the Hamiltonian (2.19), which has the permutation symmetry of the quantities αw_1 , αw_2 and α , where $\alpha = (|w_1|^2 + |w_2|^2 + 1)^{-\frac{1}{2}}$.

Without loss of generality, we study the twin-condensate sub-regime under the restriction $w_1 = w_2$, because the invariant surfaces in (2.23) are dynamically equivalent. Applying this condition to the coherent states in (2.17), we obtain:

$$\begin{aligned} |N; w_1 = w_2\rangle &= \frac{1}{\sqrt{N!}} \left[\frac{w_1 a_1^\dagger + w_1 a_2^\dagger + a_3^\dagger}{\sqrt{2|w_1|^2 + 1}} \right]^N |0\rangle \\ &= \sum_{m_1+m_2=N} \frac{\sqrt{N!}}{m_1!m_2!} \frac{(w_1 a_1^\dagger + w_1 a_2^\dagger)^{m_1} (a_3^\dagger)^{m_2}}{(2|w_1|^2 + 1)^{\frac{N}{2}}} |0\rangle. \end{aligned} \quad (3.1)$$

Now it is convenient to change the basis of the single-particle Hilbert space. Such transformation may be described by the following linear combinations of the bosonic operators:

$$\begin{cases} b_1^\dagger = \frac{a_1^\dagger + a_2^\dagger}{\sqrt{2}} \\ b_2^\dagger = a_3^\dagger \\ b_3^\dagger = \frac{a_1^\dagger - a_2^\dagger}{\sqrt{2}} \end{cases} \quad (3.2)$$

The operator b_1^\dagger (b_3^\dagger) creates a particle in the equiprobable superposition of the local states $|u_1\rangle$ and $|u_2\rangle$ arranged with identical (opposite) phases. So b_1^\dagger is responsible for the occupation of the twin-condensates, while b_2^\dagger represents the *solitary mode*, which is characterized by the single-particle state $|u_3\rangle$. Note that b_3^\dagger is also the creation operator in the state $|e_3\rangle$, found in (2.3). Applying the transformation (3.2) in (3.1), we have:

$$\begin{aligned} |N; w_1 = w_2\rangle &= \sum_{m_1+m_2=N} \left(\frac{N!}{m_1!m_2!} \right)^{\frac{1}{2}} \frac{(\sqrt{2}w_1)^{m_1} |m_1, m_2, 0\rangle}{(2|w_1|^2 + 1)^{\frac{N}{2}}} \\ &= \frac{1}{\sqrt{N!}} \left[\frac{(\sqrt{2}w_1)b_1^\dagger + b_2^\dagger}{\sqrt{2|w_1|^2 + 1}} \right]^N |0\rangle = |N; \sqrt{2}w_1\rangle_{\text{su}(2)}. \end{aligned} \quad (3.3)$$

The set of states $\{|m_1, m_2, m_3\rangle\}$ constitutes a new basis for the bosonic Fock space, where m_j represents the eigenvalue of the number operator $b_j^\dagger b_j$. Note that the SU(3) coherent state restricted to the subspace twin-condensates has no occupation in the mode related to the operator $b_3^\dagger b_3$, also called the *opposite phase mode*, evidencing the phase equality between the twin-condensates in the classical dynamics. Besides, the coherent state (3.3) is also a SU(2) coherent state with complex coordinate $\sqrt{2}w_1 = e^{-i\phi} \tan \frac{\theta}{2}$, indicating that the invariant surface of twin-condensates is topologically isomorphic to the unit sphere (S^2) [15].

The states with zero mean occupation in the opposite phase mode, given by $\langle \psi | b_3^\dagger b_3 | \psi \rangle = 0$ or $|\psi\rangle = \sum_{m_1+m_2=N} c_{m_1, m_2} |m_1, m_2, 0\rangle$ with $c_{m_1, m_2} \in \mathbb{C}$, satisfy the following

identities:

$$\begin{aligned}
 \langle \psi | a_1^\dagger a_1 + a_2^\dagger a_2 | \psi \rangle &= \langle \psi | a_1^\dagger a_2 + a_2^\dagger a_1 | \psi \rangle; \\
 \langle \psi | a_1^\dagger a_1 | \psi \rangle &= \langle \psi | a_2^\dagger a_2 | \psi \rangle; \\
 \frac{d}{dt} \langle \psi | Q_1 | \psi \rangle &= 0.
 \end{aligned} \tag{3.4}$$

Therefore, the quantum dynamics preserves the population equality between the twin-condensates, because the average of the population imbalance operator Q_1 remains zero during the quantum evolution for all the initial states in the subspace generated by the basis $\{|m_1, m_2, 0\rangle\}$. However, the quantum dynamics does not preserve the identical phases of twin-condensates, unlike the classical dynamics, because the average of $b_3^\dagger b_3$ does not remain constant, in spite of its initial zero value.

At this point it is interesting to define the generators of another subalgebra of $\mathfrak{su}(3)$ isomorphic to $\mathfrak{su}(2)$, but related to the modes present in the twin-condensate sub-regime:

$$S_x = \frac{b_1^\dagger b_2 + b_2^\dagger b_1}{2}, \quad S_y = i \frac{b_2^\dagger b_1 - b_1^\dagger b_2}{2}, \quad S_z = \frac{b_1^\dagger b_1 - b_2^\dagger b_2}{2}. \tag{3.5}$$

Now, employing the identities (3.4), we can show that:

$$\langle \psi | S_z | \psi \rangle = \frac{1}{2} \langle \psi | a_1^\dagger a_1 + a_2^\dagger a_2 - a_3^\dagger a_3 | \psi \rangle. \tag{3.6}$$

Thus, S_z is the population imbalance operator between the twin-condensates and the solitary mode, but only if the average occupation of the opposite phase mode is zero.

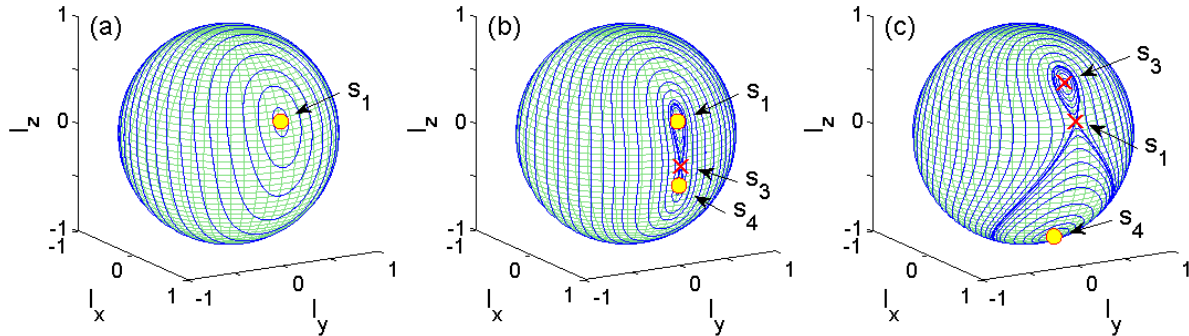


Figure 3. [colour] Classical trajectories in the invariant subspace of twin-condensates $w_1 = w_2 = \frac{1}{\sqrt{2}} e^{-i\phi} \tan \frac{\theta}{2}$ for $N = 30$, $|\Omega| = 1$, $\mu = 0$ and self-collision parameter values: (a) $\chi = 1.5$, (b) $\chi = 1.98$ and (c) $\chi = 3$. The [yellow] circles ([red] crosses) indicate the location of stable (unstable) fixed points with respect to the complete four-dimensional phase space of the three-mode condensate. The angles ϕ and θ are similar to the usual spherical coordinate angles, except that, for convenience, we take the origin of θ along the *negative* z-axis.

Figure 3 displays the classical dynamics of the three-mode model in the invariant subspace of twin-condensates, which is represented by the unit sphere, for various values of the self-collision rate χ , but neglecting the presence of cross-collisions. Observe that

the Cartesian coordinates directly represent the normalized classical averages of the SU(2) generators:

$$\begin{cases} I_x = \frac{2}{N} \langle N; w_1 = w_2 | S_x | N; w_1 = w_2 \rangle = \sin \theta \cos \phi \\ I_y = \frac{2}{N} \langle N; w_1 = w_2 | S_y | N; w_1 = w_2 \rangle = \sin \theta \sin \phi \\ I_z = \frac{2}{N} \langle N; w_1 = w_2 | S_z | N; w_1 = w_2 \rangle = -\cos \theta \end{cases} \quad (3.7)$$

Figure 3.(a), for $\chi = 1.5 < \chi_+(\mu = 0) \approx 1.971$, shows the classical dynamics in the absence of the equilibrium points s_3 and s_4 . Note that all orbits surround the stable equilibrium point s_1 and, therefore, the population imbalance varies around the value $I_z(w_1 = w_2 = 1) = \frac{1}{3}$, which represents an identical average population in all three local modes. Thus, there is no preferential occupation of any local mode, and this behaviour characterizes the dynamical regime known as *Josephson oscillation* (JO). In figure 3.(b) we show the classical dynamics for $\chi = 1.98$, i.e., a self-collision rate value slightly higher than the critical bifurcation parameter. The bifurcation is accompanied by the appearance of a *separatrix*, which crosses the unstable equilibrium point s_3 . The separatrix is the boundary between the orbits of the JO regime and the trajectories around the new stable equilibrium point s_4 . The trajectories near s_4 vary around negative values of I_z , indicating a preferential occupation of the third well. Therefore, the tunneling between twin-condensates and solitary mode is suppressed, giving rise to the effect known as *macroscopic self-trapping* (MST). The JO and MST sub-regimes are also present in the double-well model, whose classical approximation with SU(2) coherent states is quite similar to the dynamics of twin-condensates [16].

Figure 3.(c) displays the dynamics of twin-condensates for $\chi = 3$, a parameter value significantly higher than χ_+ . For $\chi > \frac{9}{4}$ the fixed point s_1 becomes unstable and takes the place of s_3 in the separatrix. Although the orbits around s_3 in the subspace of twin-condensates are regular, we should note that this equilibrium point is not a stable center in the complete phase space, since s_3 behaves like a saddle point in the directions orthogonal to the surface $w_1 = w_2$. Therefore, the self-trapping dynamics which favors the occupation of the twin-condensates, characterized by the regular trajectories with $I_z > \frac{1}{3}$ in the vicinity of s_3 , is restricted to the invariant surface. Besides, we observe that an increase in self-collision rate is accompanied by an expansion of the region on S^2 occupied by MST orbits.

Figure 4 shows the effect of cross-collisions on the dynamics of the mean population imbalance I_z for the initial coherent state $|N, w_1 = w_2 = 0\rangle = |0, 0, N\rangle$, corresponding to the south pole in figure 3. The solid [blue] (dashed [green]) curve in figure 4.(a) displays the classical time evolution of I_z for $N = 30$, $|\Omega| = 1$, $\chi = 4$ and $\mu = \frac{\chi}{100}$ ($\mu = \frac{\chi}{10}$). Notice that the greater value of the cross-collision parameter inhibits the MST, due to its correspondent increase of the effective tunneling rate $\Omega' = \Omega(1 + 2\mu)$. Therefore, the condensate dynamics can be completely changed by the cross-collisions, even when the collision parameters μ and χ have different magnitudes.

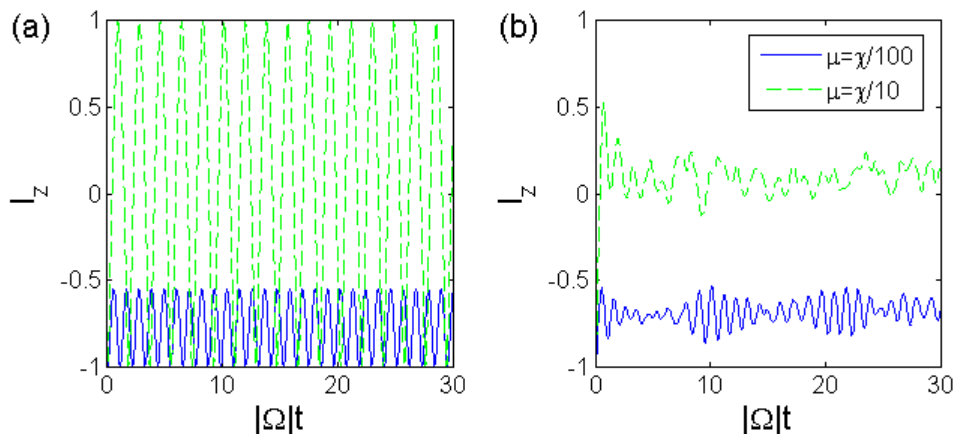


Figure 4. [colour] Left (right) figure shows the classical (quantum) time evolution of the population imbalance I_z for the initial state $|N, w_1 = w_2 = 0\rangle = |0, 0, N\rangle$. The solid [blue] (dashed [green]) curve displays the results for $N = 30$, $|\Omega| = 1$, $\chi = 4$ and $\mu = \frac{\chi}{100}$ ($\mu = \frac{\chi}{10}$).

Figure 4.(b) exhibits the quantum time evolution of I_z for a direct comparison with the classical results. Note that, unlike previous classical results, the amplitude of quantum oscillations does not remain constant during the evolution of the condensate, evidencing a quantitative disagreement between the two approaches. However, the solid [blue] (dashed [green]) curve properly characterizes the MST (JO) regime, because the fluctuations in the population imbalance remain around $I_z < 0$ ($I_z = \frac{1}{3}$). Consequently, the qualitative agreement between the classical and quantum approaches persists, even for a number of particles as small as $N = 30$.

3.1.1. Generalized Purity associated with the su(3) algebra The classical equations of motion (2.21) do not depend on the total number of trapped bosons, since they represent the dynamics in the macroscopic limit $N \rightarrow \infty$. Therefore, the qualitative agreement between the two approaches would not be expected for a small number of particles such as $N = 30$, unlike observed in figure 4. Although mean field and classical theories are quite common in the treatment of condensate dynamics, little is known about the quality of these approximations with respect to the exact quantum calculation for a microscopic or mesoscopic condensate. The classical dynamics is almost exact for a macroscopic number of particles, but for a mesoscopic or microscopic number of bosons we must be able to evaluate *quantitatively* the quality of our approximations as a function of N and the propagation time, because in an usual experiment the number of condensate particles can range from a few hundred to the order of 10^{10} bosons [17].

Our classical approximation consists of restricting the system time evolution to the nonlinear subspace of coherent states. However, the exact quantum dynamics for few particles can promote the departure of an initial coherent state from the classical subspace, thus introducing quantitative errors in our approximation. The generalized purity associated with the su(3) algebra, which is a measure capable of quantifying the

proximity of a given N -particle state $|\psi\rangle$ to the classical subspace, is given by [12]:

$$\mathcal{P}_{\text{su}(3)}(|\psi\rangle) = \frac{9}{N^2} \left(\frac{\langle \psi | Q_1 | \psi \rangle^2}{3} + \frac{\langle \psi | Q_2 | \psi \rangle^2}{4} + \sum_{j=1}^3 \frac{\langle \psi | P_j | \psi \rangle^2}{12} + \sum_{j=1}^3 \frac{\langle \psi | J_j | \psi \rangle^2}{12} \right). \quad (3.8)$$

The generalized purity is limited to the interval $0 \leq \mathcal{P}_{\text{su}(3)}(|\psi\rangle) \leq 1$, but we have $\mathcal{P}_{\text{su}(3)}(|\psi\rangle) = 1$ if and only if $|\psi\rangle$ is a coherent state. On the other hand, the value of $\mathcal{P}_{\text{su}(3)}(|\psi\rangle)$ is decreasing with the “distance” of $|\psi\rangle$ to the subspace of coherent states. Therefore, $\mathcal{P}_{\text{su}(3)}(|\psi\rangle)$ is a *classicality* measure, because the purity value is increasing with the classical character of $|\psi\rangle$, taking the coherent states as the most classical pure states, due to their minimum uncertainty on the phase space.

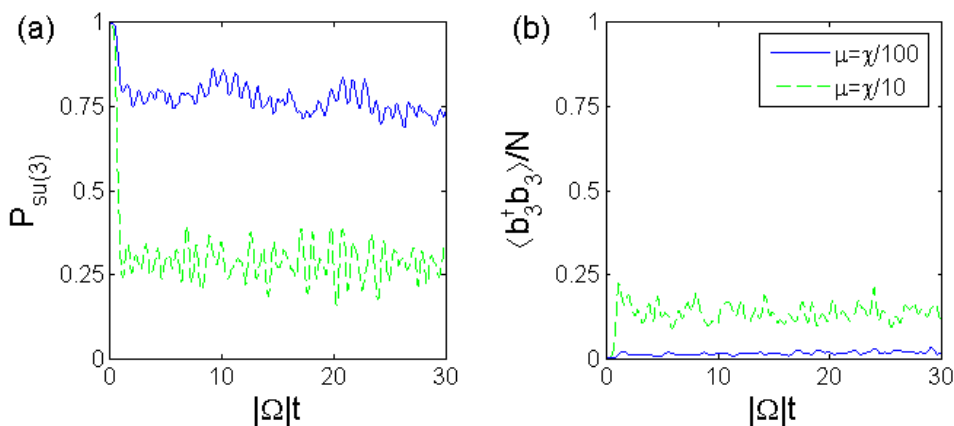


Figure 5. [colour] Left (right) figure shows the time evolution of $\mathcal{P}_{\text{su}(3)}$ ($\langle b_3^\dagger b_3 \rangle$) for an immediate comparison with the figure 4. The solid [blue] (dashed [green]) curve shows the results for $N = 30$, $|\Omega| = 1$, $\chi = 4$, $\mu = \frac{\chi}{100}$ ($\mu = \frac{\chi}{10}$) and initial state $|N, w_1 = w_2 = 0\rangle = |0, 0, N\rangle$.

Figure 5.(a) displays the evolution of $\mathcal{P}_{\text{su}(3)}$ for the same initial state and parameters of figure 4. Note that the state initially suffers a sudden purity loss, which is responsible for the quantitative disagreement between the classical and quantum results. Therefore, only for a very short time interval the classical approximation roughly coincides with the quantum dynamics, when considering a small number of particles. However, after a brief initial period of purity loss, $\mathcal{P}_{\text{su}(3)}$ only exhibits fluctuations around a stable value. The purity loss in the MST regime is inferior to the JO regime, indicating the better quality of the classical approximation in the self-trapping dynamics. The orbits associated with the JO regime traverse a larger region of the phase space compared with the localized MST trajectories, as shown in figure 3. Therefore, the quantum states related to the JO regime have greater delocalization (uncertainty) on the phase space, which is responsible for their accentuated classicality loss.

Within the classical approximation, the invariant subspaces of twin-condensates are defined by the equality of phase and mean occupation between two local modes. Although the quantum dynamics preserves the population equality between identical local condensates, according to the equation (3.4), the phase difference does not remain

zero. In general, using the transformation (3.2) in the Hamiltonian (2.8), we can show that:

$$\frac{d}{dt}\langle N; w_1 = w_2 | b_3^\dagger b_3 | N; w_1 = w_2 \rangle \neq 0. \quad (3.9)$$

Except for $\chi = \mu = 0$ or $N \rightarrow \infty$, when the classical approximation is exact. Therefore, the subspaces with no phase difference between two local modes are not quantum invariant. The population dynamics of the opposite phase mode for the states $|N, w_1 = w_2\rangle$ can not be described classically, and therefore it represents a process of purity (classicality) loss. Figure 5.(b) shows the behaviour of $\langle b_3^\dagger b_3 \rangle$ for the same initial state and parameters of the previous figure. In comparison with the figure 5.(a), we observe that a higher occupation of the opposite phase mode is accompanied by a greater purity loss. Therefore, the nonzero occupation of the opposite phase mode is partially responsible for breaking the quantum-classical correspondence in the sub-regime of twin-condensates. Moreover, the quantity $\langle b_3^\dagger b_3 \rangle$ can be used as a measure of validity (quality) of the classical approximation in the invariant subspaces.

3.2. Single Depleted Well Dynamics

The sub-regime of twin-condensates is very similar to the dynamics of a condensate in a double-well potential, since both models have several features in common, such as the integrability, the SU(2) coherent states, and especially the dynamical transition from JO to MST. Therefore, the single depleted well states (SDWS) represent the first example of an entirely new population dynamics for the three-mode model.

According to the transformation (2.22), the SDWS have a completely empty local mode, while the two other modes remain with the same mean occupation and opposite phases. Similarly to the self-trapping regime, the SDWS represent a dynamical effect of tunneling suppression, but the opposite phases between the preferentially occupied local modes distinguish the latter regime.

Due to the rotational symmetry of the trapping potential, all the SDWS are equivalent. Thus, without loss of generality, we restrict our results to the region of phase space in the vicinity of $(w_1 = -1, w_2 = 0)$, where the second local mode is empty.

The SDWS have fixed positions in the phase space, but their stability varies as a complicated function of the collision parameters χ and μ , according to the condition (2.29) and the figure 2.(b). Figure 6.(a) shows the Poincaré section at $\phi_2 = 0$ for $\chi = 5$ and $\mu = \frac{\chi}{100}$, considering only the trajectories with the same energy of the SDWS. Note that the section presents the stable SDWS located in the center of a bundle of regular orbits. The energetically accessible region of phase space is filled by orbits with a behaviour similar to the SDWS, since they exhibit only small fluctuations in the average occupation of the second local mode, while the other two modes oscillate in opposite phase around $\frac{N}{2}$.

Figure 6.(b) shows the Poincaré section in the vicinity of the SDWS for $\chi = -5$ and $\mu = \frac{\chi}{100}$. Here we see an unstable SDWS inserted in a chaotic region of phase space. We

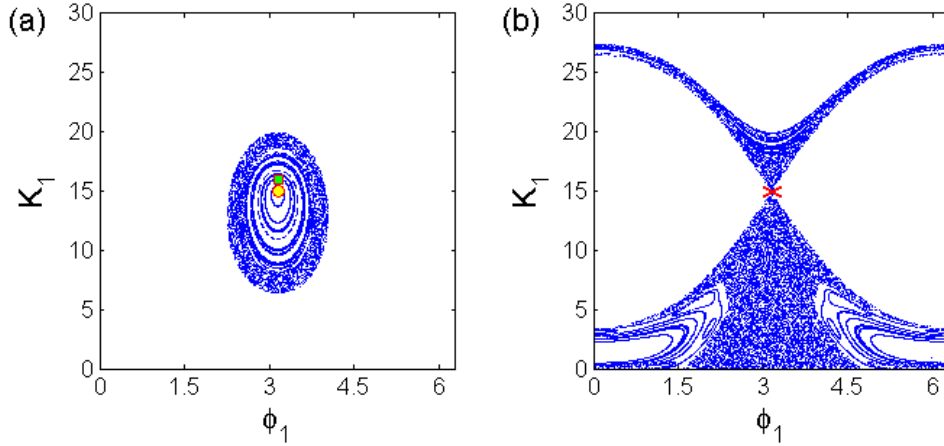


Figure 6. [colour] Left (right) figure shows the Poincaré section at $\phi_2 = 0$ for $N = 30$, $|\Omega| = 1$, $\chi = 5$ ($\chi = -5$), $\mu = \frac{\chi}{100}$, considering only those trajectories with the same energy of the fixed point ($w_1 = -1, w_2 = 0$). The [yellow] circle ([red] cross) shows the position of the stable (unstable) equilibrium point in the section.

also observe that the SDWS is the boundary between two distinct sets of chaotic orbits, because the trajectories above (below) the equilibrium point in this section preserve the condition $K_1 > \frac{N}{2}$ ($K_1 < \frac{N}{2}$) during their time evolution. Unlike the stable case, the energetically accessible region of phase space in the vicinity of the fixed point does not show a behaviour similar to the SDWS, since there is no persistent depletion of the second local mode.

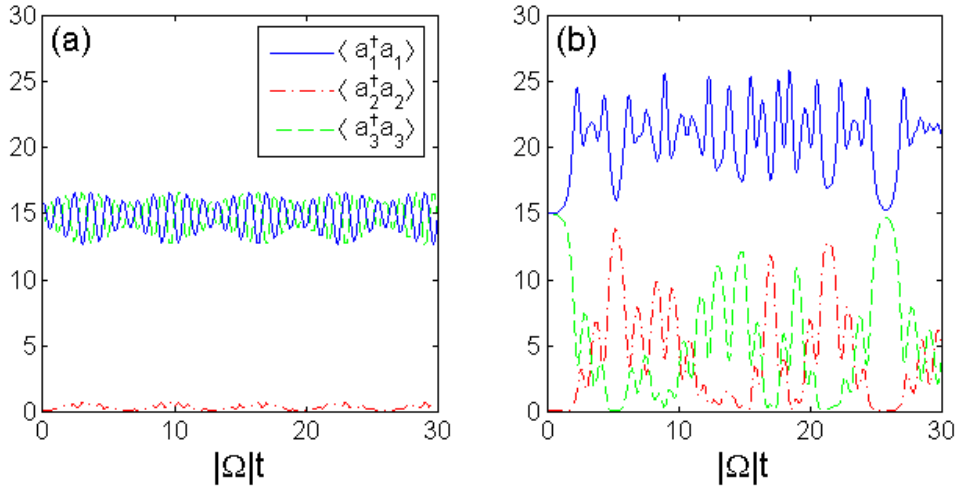


Figure 7. [colour] Left (right) figure shows the classical population dynamics for an initial condition near one of the SDWS, considering $N = 30$, $|\Omega| = 1$, $\chi = 5$ ($\chi = -5$), $\mu = \frac{\chi}{100}$.

The regular population dynamics in the vicinity of the SDWS for $\chi = 5$ and $\mu = \frac{\chi}{100}$ is illustrated in figure 7.(a), employing the initial condition indicated by the square [green] marker in figure 6.(a). As expected, the second local mode remains almost empty, while the two remaining modes exhibit periodic population inversions around

$\frac{N}{2}$. Figure 7.(b) shows the chaotic population dynamics for $\chi = -5$ and $\mu = \frac{\chi}{100}$, given an initial condition very close to the SDWS with $K_1 > \frac{N}{2}$. Note that the second local mode does not remain empty, and it presents successive population inversions with the third mode, while the first mode holds more than half of the trapped bosons.

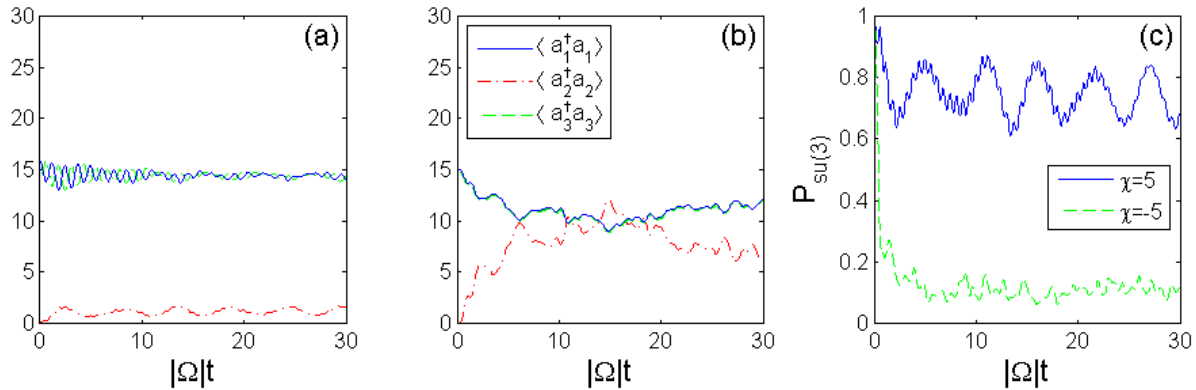


Figure 8. [colour] Left (center) figure shows the quantum evolution of the average occupations in the three local modes for $N = 30$, $|\Omega| = 1$, $\chi = 5$ ($\chi = -5$), $\mu = \frac{\chi}{100}$, considering as the initial state the coherent state centered at the initial condition of the trajectory in figure 7.(a) (figure 7.(b)). Notice in (b) that the curves for $\langle a_1^\dagger a_1 \rangle$ and $\langle a_3^\dagger a_3 \rangle$ are almost superimposed. The solid [blue] and dashed [green] curves in (c) represent the dynamics of $\mathcal{P}_{\text{su}(3)}$ corresponding to the results displayed in (a) and (b), respectively.

For direct comparison with the previous classical results, the exact quantum population dynamics is shown in figure 8, where we used as initial states the coherent states centered at the initial conditions of figure 7. Figure 8.(a) displays the quantum population dynamics corresponding to the regular trajectory near the SDWS. The mean occupation in the second local mode is slightly higher than in the classical approximation, but the preferential occupation in the other two modes still prevails. Therefore, there is a fair agreement between the exact quantum result and the classical approximation when we consider a regular orbit close to the stable SDWS. However, the quantum dynamics corresponding to the chaotic trajectory, shown in figure 8.(b), has little resemblance to its classical analogue. Unlike the classical approximation, there is no preferential occupation of the first mode, which displays values below $\frac{N}{2}$. On the other hand, the second well does not remain empty, as expected for the irregular dynamics near the SDWS.

The dynamics of $\mathcal{P}_{\text{su}(3)}$ confirms that the classical approximation is more accurate for the regular trajectory, as we see in figure 8.(c). The state associated with the chaotic dynamics has a large purity loss, which corresponds to a large delocalization in the phase space. Conversely, the time evolution of the state under the regular dynamics preserves its similarity to the coherent states, i.e., the state remains well localized in the phase space and exhibits relatively high values of purity during its evolution.

3.3. Vortex Dynamics

The vortex states are the only equilibrium points of the classical approximation with nonzero imaginary parts. Thus, they are the only ones with nonzero angular momentum along the symmetry axis of the trapping potential. To emphasize the imaginary parts of the complex variables w_j during their time evolution, we introduce a new set of canonical variables:

$$w_j = \frac{q_j + ip_j}{\sqrt{2N - q_1^2 - p_1^2 - q_2^2 - p_2^2}}. \quad (3.10)$$

The real variables q_j and p_j are directly related to the real and imaginary parts of w_j , respectively. Note also that these new dynamical variables must satisfy the condition $2N \geq q_1^2 + p_1^2 + q_2^2 + p_2^2$. We show below only the results for the vortex state parametrized by $w_1 = e^{i\frac{2\pi}{3}} = w_2^*$, since the two vortex states differ only by the sense of rotation, as previously discussed.

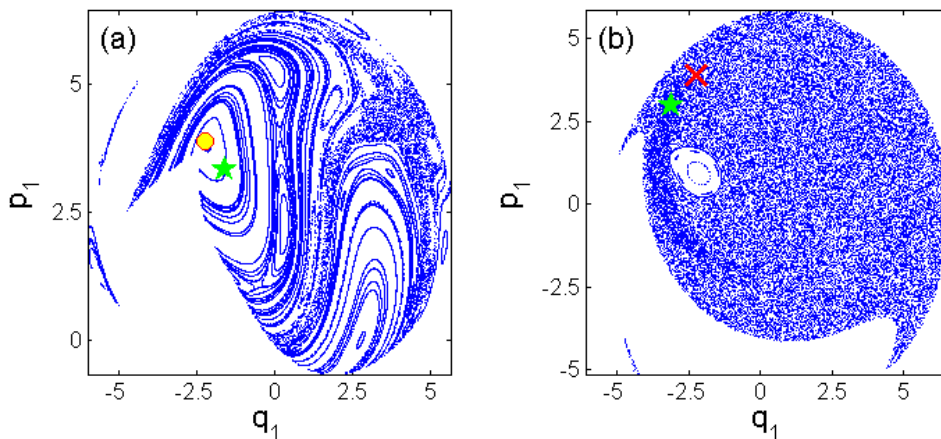


Figure 9. [colour] Left (right) figure shows the Poincaré section at $p_2 = -\sqrt{N}/2$ for $N = 30$, $|\Omega| = 1$, $\chi = -1$ ($\chi = -5$) and $\mu = \frac{\chi}{100}$, considering only those trajectories with the same energy of the vortex state $w_1 = e^{i\frac{2\pi}{3}} = w_2^*$. The stable (unstable) equilibrium point is represented by the [yellow] circle ([red] cross).

Figure 9 shows the dynamics in the vicinity of the vortex state for two completely different situations. For $\chi = -1$ and $\mu = \frac{\chi}{100}$ the Poincaré section at $p_2 = -\sqrt{N}/2$ displays the stable vortex state in a regular region of phase space. However, for $\chi = -5$ and $\mu = \frac{\chi}{100}$, the vortex state is unstable and the dynamics of the system is almost completely chaotic.

According to the equation (2.15), the angular momentum of the condensate along the symmetry axis of the trapping potential is directly proportional to the $\text{su}(3)$ operator $J_S = J_1 + J_2 + J_3$. Therefore, the rotational dynamics of the condensate is illustrated in Figure 10, where we consider the initial conditions indicated by the [green] star markers in figure 9. The solid [blue] (dashed [green]) curve in figure 10.(a) shows the classical dynamics of a regular (chaotic) trajectory near the vortex state. Note that only the regular trajectory represents a persistent collective rotation of the condensate.

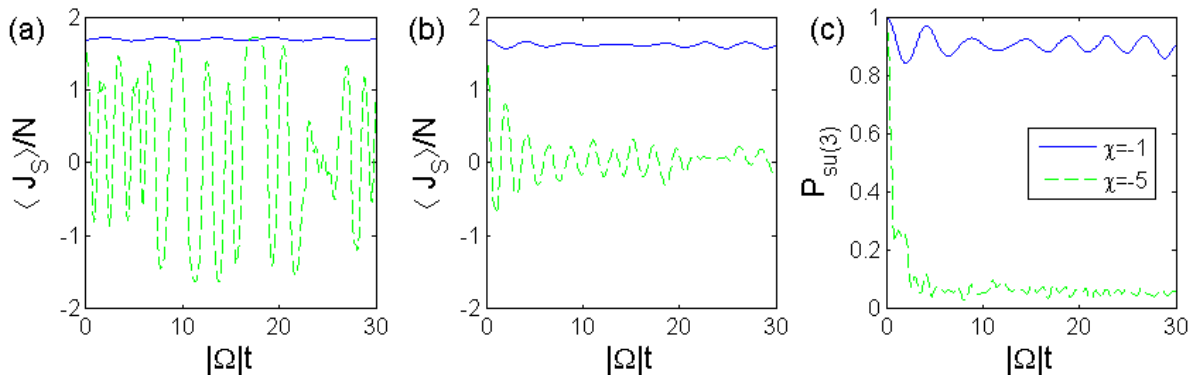


Figure 10. [colour] Left (middle) figure exhibits the classical (quantum) dynamics of $\langle J_S \rangle$, quantity directly proportional to the angular momentum of the condensate along the symmetry axis of the trapping potential. The solid [blue] (dashed [green]) curve shows the time evolution for $N = 30$, $|\Omega| = 1$, $\chi = -1$ ($\chi = -5$), $\mu = \frac{\chi}{100}$ and the initial condition indicated by the [green] star marker in figure 9.(a) (figure 9.(b)). Right figure shows the dynamics of $\mathcal{P}_{\text{su}(3)}$ for the same initial conditions.

Therefore, the rotation of the condensate in a preferential sense is present only when the vortex state is stable. The chaotic trajectory does not exhibit preferential sense of rotation, but presents oscillations of angular momentum with large amplitudes. However, the maximum value of $\langle J_S(t) \rangle$ in both trajectories remains bounded by $\sqrt{3}N$, which corresponds to the mean value of J_S for the vortex state, according with (2.32).

Figure 10.(b) shows the quantum dynamics of rotation, where we consider the initial coherent states centered on the initial conditions of figure 10.(a). Note that even for $N = 30$, a relatively small number of trapped bosons, the quantum results of $\langle J_S(t) \rangle$ associated with the regular trajectory demonstrate good agreement with the classical approximation. However, in the chaotic case, the amplitude of the oscillations are strongly attenuated. Thus, as expected, the approximation is not quantitatively satisfactory in the chaotic regime, although the absence of a preferential sense of rotation is evidenced in both approaches. Figure 10.(c) displays the dynamics of $\mathcal{P}_{\text{su}(3)}$ for the two orbits previously selected. Note that the purity loss in the chaotic regime is much faster and more intense when compared to the regular system, confirming the differences found in the precision of the classical approximation.

4. Conclusion

In the present work, we have investigated the quantum dynamics of a Bose-Einstein condensate confined in a symmetric triple-well potential employing an approximation based on the TDVP and the SU(3) coherent states. We have exploited maximally the use of coherent states as initial states chosen to be centered in appropriate points of the classical manifold, particularly near the equilibrium points of the classical equations of motion. This scheme allowed us to capture in the complete quantum calculations some of the particularities of the classical solutions.

Moreover, in order to evaluate the quality of the classical Hamiltonian evolution, as compared to the quantum results, we employed the purity associated with the $\text{su}(3)$ algebra. The generalized purity measures the departure from the subspace of coherent states, in which our classical approximation is restricted, thus enabling us to quantify the quality of the approximation. The classical approximation quality depends not only on the total number of particles, but also on the location in phase space of the initial coherent state and the regularity of the Hamiltonian flow in its vicinity. We concluded that even for a relatively small number of particles such as $N = 30$, which is very far from the classical-macroscopic limit, the classical results obtained for the *regular* dynamical regime display a fair agreement with the quantum time evolution, unlike the *chaotic* regime.

Considering the sub-regime of *twin-condensates*, we have shown that the self-trapping dynamics may be suppressed by the cross-collisions effects on the effective tunneling rate, which can become quite important for a large number of trapped bosons. Since this sub-regime is classically integrable, its classical approximation exhibits excellent results. Whereas, the *single depleted well* regime, which is characterized by the complete depletion of a local mode, can be effectively eliminated in phase space when its corresponding fixed points become unstable, giving way to chaos. In the chaotic regime, a single Hamiltonian trajectory clearly does *not* account for the quantum dynamics of an initial coherent state at long times. This fact is precisely indicated by the generalized purity. In the same line of reasoning, the persistent collective rotation in a preferential sense, presented in the vicinity of the *vortex* states in phase space, can only be properly observed when the corresponding fixed points are stable.

Acknowledgments

T.F.V. would like to thank Marcus A. M. de Aguiar for many insightful discussions. We also acknowledge the financial support from FAPESP under Grant No. 2008/09491-9 and CNPq under Grant No. 304041/2007-6. This work is partially supported by the Brazilian National Institute of Science and Technology of Quantum Information (INCT-IQ).

References

- [1] Parkins A S and Walls D F 1998 *Phys. Rep.* **303** 1–80
Dalfovo F, Giorgini S, Pitaevskii L and Stringari S 1999 *Rev. Mod. Phys.* **71** 463–512
Cornell E A and Wieman C E 2002 *Rev. Mod. Phys.* **74** 875–93
- [2] Milburn G J, Corney J, Wright E M and Walls D F 1997 *Phys. Rev. A* **55** 4318–24
Smerzi A, Fantoni S, Giovanazzi S and Shenoy S R 1997 *Phys. Rev. Lett.* **79**, 4950–53
- [3] Hines A P, McKenzie R H and Milburn G J 2003 *Phys. Rev. A* **67** 013609
Sanz L, Angelo R M and Furuya K 2003 *J. Phys. A: Math. Gen.* **36** 9737–54
- [4] Viscondi T F, Furuya K and de Oliveira M C 2009 *Phys. Rev. A* **80** 013610
- [5] de Oliveira M C and da Cunha B R 2009 *Int. J. Mod. Phys. B* **23**, 5867–80
- [6] Buonsante P, Franzosi R and Penna V 2003 *Phys. Rev. Lett.* **90** 050404

- Buonsante P, Franzosi R and Penna V 2004 *Laser Physics* **14** 556–64
- Mossmann S and Jung C 2006 *Phys. Rev. A* **74** 033601
- Liu B, Fu L-B, Yang S-P and Liu J 2007 *Phys. Rev. A* **75** 033601
- [7] Nemoto K, Holmes C A, Milburn G J and Munro W J 2000 *Phys. Rev. A* **63** 013604
- Franzosi R and Penna V 2001 *Phys. Rev. A* **65** 013601
- Franzosi R and Penna V 2003 *Phys. Rev. E* **67** 046227
- [8] Furuya K, Nemes M C and Pellegrino G Q 1998 *Phys. Rev. Lett.* **80** 5524
- [9] Kramer P and Saraceno M 1980 *Geometry of the Time-Dependent Variational Principle in Quantum Mechanics (Lecture Notes Physics vol 140)* (New York: Springer-Verlag)
- Zhang W-M, Feng D H, Yuan J-M and Wang S-J 1989 *Phys. Rev. A* **40** 438–47
- Zhang W-M, Feng D H and Yuan J-M 1990 *Phys. Rev. A* **42** 7125–50
- [10] Perelomov A M 1986 *Generalized Coherent States and their Applications* (Berlin: Springer-Verlag)
- Raghunathan K, Seetharaman M and Vasani S S 1989 *J. Phys. A: Math. Gen.* **22**, L1089–92
- Zhang W-M, Feng D H and Gilmore R 1990 *Rev. Mod. Phys.* **62** 867–927
- Mathur M and Sen D 2001 *J. Math. Phys.* **42** 4181
- [11] Visconti T F, Furuya K and de Oliveira M C 2010 *EPL* **90** 10014
- [12] Klyachko A A 2002 Coherent states, entanglement, and geometric invariant theory *Preprint* quant-ph/0206012v1.
- Somma R, Ortiz G, Barnum H, Knill E and Viola L 2004 *Phys. Rev. A* **70** 042311
- Barnum H, Knill E, Ortiz G and Viola L 2003 *Phys. Rev. A* **68** 032308
- Barnum H, Knill E, Ortiz G, Somma R and Viola L 2004 *Phys. Rev. Lett.* **92** 107902
- Delbourgo R and Fox J R 1977 *J. Phys. A: Math. Gen.* **10** L233
- Delbourgo R 1977 *J. Phys. A: Math. Gen.* **10** 1837
- [13] Pethick C J and Smith H 2002 *Bose-Einstein Condensation in Dilute Gases* (Cambridge: Cambridge University Press)
- [14] Yaffe L G 1982 *Rev. Mod. Phys.* **54** 407–35
- [15] Arecchi F T, Courtens E, Gilmore R and Thomas H 1972 *Phys. Rev. A* **6** 2211–37
- [16] Visconti T F, Furuya K and de Oliveira M C 2009 *Ann. Phys., NY* **324** 1837–46
- [17] Leggett A J 2001 *Rev. Mod. Phys.* **73** 307–56